9.4 Insights into Tornado Structure Afforded by High-frequency Mobile Radar

Christopher C. Weiss*
Texas Tech University, Lubbock, TX

Timothy Cermak,
University of Oklahoma / CIMMS, Norman, OK

Ryan Metzger[1], Anthony Reinhart[2], Patrick Skinner[3]
[1]National Weather Service, Fairbanks, AK
[2]Texas Tech University, Lubbock, TX
[3]National Severe Storms Laboratory, Norman, OK

1. INTRODUCTION

A number of recent radar studies have provided insights into the core structure of tornadoes (e.g., Lee and Wurman 2005; Tanamachi et al. 2007; Kosiba et al. 2008; Kosiba and Wurman 2010; Wakimoto et al. 2012; Tanamachi et al. 2013; Wurman et al. 2013). These studies primarily have considered the horizontal structure of tornado vortices, often with the assistance of tools such as the Ground-based Velocity Track Display (GBVTD; Lee et al. 1999) that assume a largely axisymmetric flow; some (e.g., Kosiba and Wurman 2013) have been able to use these analyses to deduce vertical variations in the tangential, radial and vertical components of tornado flow.

To date, there have been very few direct observations of the vertical secondary circulation associated with tornadoes (e.g., Bluestein et al. 2003; Bluestein et al. 2004), particularly including the (often) very-shallow tornado inflow boundary layer, which is suspected to be as shallow as the lowest 10 m above ground level (AGL). This study seeks to make these measurements utilizing the Texas Tech Ka-band radars. The high transmit frequency (35 GHz) limits the effects of diffraction and, therefore, permits a very narrow half-power beamwidth of 0.33 deg, which is critical for sampling the inflow layer to tornadoes. At typical ranges during tornado intercepts of 2 (5) km, the linear cross-beam resolution is approximately 10 m (25 m). Range resolution retrieved from non-linear pulse compression is of comparable magnitude.

* *Corresponding author address: Christopher C. Weiss, Texas Tech University, Atmospheric Science Group, Department of Geosciences, Lubbock, TX, 79409; e-mail: Chris.Weiss@ttu.edu*

2. DATA COLLECTION STRATEGY AND CASE OVERVIEW

Owing to the relative paucity of sustained significant tornadoes during the field phase of the Verification of the Origin of Rotation in Tornadoes Experiment (VORTEX2; Wurman et al. 2012), faculty and students from Texas Tech University sought additional data collection opportunities in the 2012 and 2013 spring seasons. The experimental design prioritized unobstructed looks at the near-surface contact layer for these tornadoes, such that range-height indicator (RHI) scans would be able to sample the boundary layer and corner flow regions (Lewellen 1976) without significant ground-clutter contamination.

Data collected during two events will be presented in this study. The first case is from 18 May 2013, near Rozel, KS. A slow-moving EF4 tornado (Fig. 1) touched down ~9 km to the southwest of Rozel at 0018 UTC (19 May) and propagated north-northwestward over a path of ~11 km before dissipating at 0047 UTC. TTUKa-2 was deployed for the event (TTUKa-1 was undergoing an upgrade to the reflector), and was positioned along US-183 about 9 km from the tornado. The unanticipated northward motion of the tornado unfortunately maintained approximately the same range throughout the sampling period (0024-0050 UTC). Though a few plan-position indicator scans were interweaved, the focus was primarily on obtaining RHI data.

The second case discussed is from 14 April 2012, to the west of Cherokee, OK. The tornadoes that occurred here were part of a larger outbreak over portions of Nebraska, Kansas and Oklahoma. Owing to the fast storm motion, TTUKa-1 and TTUKa-2 separated to maximize the probability of obtaining single-platform RHIs on tornadoes. TTUKa-1 began scanning at 0055 UTC (15 April) from a position west of Cherokee. During the period of operations (0055 – 0115 UTC), the storm that produced an EF1 tornado ~10 km W of Cherokee cycled to produce a new

EF0 tornado ~3 km W of Cherokee and within 2.5 km of the radar position (Fig. 2) where there was a clear line of sight to the contact point of the tornado with the ground.

3. RESULTS AND DISCUSSION

Flow within the Tornado Boundary Layer and Corner Flow Regions

RHIs through the core flow, somewhat to the outbound side, of the Rozel, KS tornado (Fig. 3a) at 0038 UTC reveal well the vertical secondary circulation. A shallow inflow boundary layer, ~50 m deep at the nearest point to the diameter of maximum wind (DMW; 700 m in this case), increasing to 200-400 m deep beyond 500 m from the DMW, transitions to outflow above this boundary layer (consider the sense of the black arrows in Fig. 3a). The structure and depth, when normalized by the DMW, compare remarkably well with the large-eddy simulations of Lewellen et al. (2000) (Fig. 3b), where the height of maximum inflow scales as 0.05 DMW and the height of maximum inflow magnitude scales as 0.2 DMW.

The asymmetric slope of the top of the boundary layer, the demarcation between inflow (below) and outflow (above), is rather unlike the Lewellen et al. 2000 simulations. On the west side of the tornado, this slope is shown to be much more inclined than the representation to the east. In fact, the boundary layer depth barely exceeds 200 m AGL out to 2 km on the east side, whereas this depth increases markedly to over 400 m AGL to the west. Lewellen (1993) identified the role of radial pressure gradients in the vertical flux divergence of radial velocity:

$$\rho \frac{\partial \overline{u'w'}}{\partial z} = \rho \frac{v^2}{r} - \frac{\partial p}{\partial r} \qquad (1)$$

where *u* is the radial velocity and *v* is the tangential velocity. From (1), it is apparent that deviations from the local cyclostrophic balance are tied to the vertical flux of radial momentum. By extension, it is suggested here that heterogeneities in pressure within the tornado inflow, for example those controlled hydrostatically by variations in buoyancy, could be tied to the observed asymmetric boundary layer depths through the forcing of the left-hand side of (1).

The second tornado from the Cherokee, OK case (the nearest to the radar) provides a radically different depiction of core flow, in this case somewhat to the inbound side of the tornado. At 0104 UTC (Fig. 4a), the flow is clearly divergent within the lowest 200 m AGL; the outbound (northwestward-moving) flow comes to a point at the surface ~2.5 km northwest of the tornado, the position of the rear-flank gust front (Fig. 4b). Storm-scale inflow is lifted above this very shallow RFD, occupying a layer from 200-600 m AGL. On the southeast side of the tornado, there is a clear indication of impingement towards the central tornado axis through this same layer. The widening of the flow above this layer in many respects looks like the profile one might expect if the ground was located at 200 m AGL; in this case, there is a strong divergent layer located beneath this corner region. The tornado at this time (0104:45 UTC; Fig. 5a) appeared to be disorganized, though still in contact with the surface. However, 105 s later (0106:30 UTC; Fig. 5b), the condensation funnel had redeveloped, indicating, all else equal, that the central core pressure had dropped, at least aloft.

Ancillary Vorticity near Tornadoes

RHIs of the first tornado from the Cherokee, OK case at 0102 UTC reveal an area of very strong (O~10^{-1} s^{-1}) vorticity. (All vorticity estimates are made using the assumption of a Rankine model, $2/r\ d(Vr)/d\phi$ in this case, where ϕ is the elevation angle.) This area is located approximately 600 m to the west of "old" tornado #1 (Fig. 6a). There are two possible explanations for this feature. On one hand, it is possible that a separate tornado existed to the west of tornado #1. However, there was no visual evidence of any condensation funnel in this region from photos and videos taken by the Texas Tech and University of Michigan teams. Considering a PPI image from 180 s after the RHI (Fig. 6b; 0105 UTC), there does appear to be a boundary along the northern fringe of a resolved internal RFD surge, with areas of weaker vertical vorticity along it. Though it is possible these areas may have aligned directly along the radial behind tornado #1 at 0102 UTC, the vorticity would have had to decrease markedly over the following 180 s, and the tilt of these vorticity centers would have had to been sharply northward, opposite of what was observed with tornado #1 at the time.

The second possibility is that the vorticity resolved is solely horizontal, in which case it is a fruitful exercise to consider its cause as such magnitudes of vorticity/tendency could be relevant to the budget of tornadoes downstream for any parcels passing through this region. The closest analog may be the baroclinic generation of horizontal vorticity owing to pseudo-horizontal gradients of air density produced by latent chilling, which at least partially drive downdraft production in the flanking regions of supercell storms. This type of vorticity generation has been considered in a number of observational and numerical studies (e.g., Rotunno and Klemp 1985; Davies-Jones and Brooks 1993; Shabbott and Markowski 2006; Skinner et al. 2011; Markowski et al. 2012; Beck and Weiss 2013; Weiss et al. 2015) as a pertinent contributor to the vorticity budget of tornadoes, usually along demarcations between inflow (with base-state thermodynamic quantities) and virtually cool outflow (e.g., within the forward-flank reflectivity gradient, along the rear-flank gust front). Without dual-Doppler data, it is impossible to identify the westernmost incursion of inflow air to the west/southwest of the RFGF (Fig. 4b), but the location relative to the RFGF and the colloquial understanding of the older member of a cycling tornado pair being occluded suggests that inflow air may well not be present near this vortex. However, the presence of an internal surge of RFD air immediately to the southeast suggests that, if this air is virtually cooler than the pre-existing RFD air on the other side of the boundary, some baroclinic tendency is possible at the location of the observed vortex. It is also worth mentioning that even if the vorticity tendency is negligible at the location of the vortex, such vorticity could be advected from upstream source regions like the RFGF, and perhaps even stretched horizontally. Unfortunately, no thermodynamic observations are available for this case to test any of these hypotheses, but the authors are currently re-examining VORTEX2 cases with “StickNet” and mobile mesonet data to see if any similar patterns emerge.

4. SUMMARY AND CONCLUSIONS

The TTUKa radars were used to intercept two tornado events, with the expressed purpose of resolving vertical tornado structure. The following conclusions are put forth from this research:

- Tornado boundary layers can be highly asymmetric, possibly due to the heterogeneity of the tornado inflow environment over the storm scale,
- Tornadoes can, at least, maintain themselves when residing above a very shallow divergent near-surface layer for a short period of time, and
- Very strong vorticity of O~10^{-1} s^{-1} is shown to exist within 500 m of an observed, likely occluded, tornado. If the vorticity is solely horizontal, it may represent a baroclinic solenoid due to pseudo-horizontal gradients of air density along the lateral edge of an internal rear-flank downdraft surge, or may be advected from other baroclinic boundaries upstream.

7. ACKNOWLEDGEMENTS

This study is funded by NSF grant AGS-0800542 and AGS-0964088. Many thanks to the faculty and students within the Texas Tech Atmospheric Science Group, Texas Tech National Wind Institute, and the University of Michigan Atmospheric, Oceanic and Space Science program for their time and talents in the field. Thanks also to Karen Kosiba, Josh Wurman and Paul Robinson (CSWR) for providing companion DOW data for the Rozel, KS case, which will be used in further study of the features discussed in this paper.

8. REFERENCES

Beck, J. R., and C. C. Weiss, 2013: An assessment of low-level baroclinity and vorticity within a simulated supercell. *Mon. Wea. Rev.*, **141**, 649-669.

Bluestein, H. B., W.-C. Lee, M. Bell, C. C. Weiss, and A. L. Pazmany, 2003: Mobile Doppler radar observations of a tornado in a supercell near Bassett, Nebraska, on 5 June 1999. Part II: Tornado-vortex structure. *Mon. Wea. Rev.*, **131**, 2968-2984.

Bluestein, H. B., C. C. Weiss, and A. L. Pazmany, 2004: The vertical structure of a tornado: High-resolution, W-band, Doppler radar observations near Happy, Texas, on 5 May 2002: *Mon. Wea. Rev.*, **132**, 2325-2337.

Davies-Jones, R. P., and H. E. Brooks, 1993: Mesocyclogenesis from a theoretical perspective. *The Tornado: Its Structure, Dynamics, Prediction, ad Hazards. Geophys. Monogr.*, Vol. 79, Amer. Geophys. Union, 105-114.

Kosiba, K. A., and J. Wurman, 2010: The three-dimensional axisymmetric structure of the Spencer, South Dakota, 1998, tornado. *J. Atmos. Sci.*, **67**, 3074-3083.

Kosiba, K. A., and J. Wurman, 2013: The three-dimensional structure and evolution of a tornado boundary layer. *Wea. Forecasting*, **28**, 1552-1561.

Kosiba, K. A., R. J. Trapp, and J. Wurman, 2008: An analysis of the axisymmetric three-dimensional low-level wind field in a tornado using mobile radar observations. *Geophys. Res. Lett.*, **35**, L05805.

Lee, W.-C., and J. Wurman, 2005: Diagnosed three-dimensional axisymmetric structure of the Mulhall tornado on 3 May 1999. *J. Atmos. Sci.*, **62**, 2373-2393.

Lee, W.-C., B. J.-D. Jou, P.-L. Chang, and S.-M. Deng, 1999: Tropical cyclone kinematic structure retrieved from single-Doppler radar observations. Part I: Doppler velocity patterns and the GBVTD technique. *Mon. Wea. Rev.*, **127**, 2419-2439.

Lewellen, W.S., 1976: Theoretical models of the tornado vortex. Proceedings of Symposium on Tornadoes: Assessment of Knowledge and Implications for Man, Lubbock, TX, Texas Tech University, pp.107-143.

Lewellen, W. S., 1993: Tornado vortex theory. *The Tornado: Its Structure, Dynamics, Prediction and Hazards*, C. Church, D. Burgess, C. Doswell, and R. Davies-Jones, Eds., American Geophysical Union.

Lewellen, D. C., W. S. Lewellen, and J. Xia, 2000: The influence of a local swirl ratio on tornado intensification near the surface. *J. Atmos. Sci.*, **57**, 527-544.

Markowski, P. M., Y. Richardson, J. Marquis, R. Davies-Jones, J. Wurman, K. Kosiba, P. Robinson, E. Rasmussen, D. Dowell, 2012: The pretornadic phase of the Goshen County, Wyoming, supercell of 5 June 2009 intercepted by VORTE2. Part II: Intensification of low-level rotation. *Mon. Wea. Rev.*, **140**, 2916-2938.

Rotunno, R. and J. Klemp, 1985: On the rotation and propagation of simulated supercell thunderstorms. *J. Atmos. Sci.*, **42**, 271-292.

Shabbott, C. J. and P. M. Markowski, 2006: Surface in situ observations within the outflow of forward-flank downdrafts of supercell thunderstorms. *Mon. Wea. Rev.*, **134**, 1422-1441.

Skinner, P. S., C. C. Weiss, J. L. Schroeder, L. J. Wicker, and M. I. Biggerstaff, 2011: Observations of the surface boundary structure within the 23 May 2007 Perryton, Texas supercell. *Mon. Wea. Rev.*, **139**, 3730-3749.

Tanamachi, R. L., H. B. Bluestein, W.-C. Lee, M. Bell, and A. Pazmany, 2007: Ground-based velocity display (GBVTD) analysis of W-band Doppler radar data in a tornado near Stockton, KS, on 15 May 1999. *Mon. Wea. Rev.*, **135**, 783-800.

Tanamachi, R. L., H. B. Bluestein, M. Xue, W.-C. Lee, K. A. Orzel, S. J. Frasier, R. M. Wakimoto, 2013: Near-surface vortex structure in a tornado and in a sub-tornado-strength convective-storm vortex observed by a mobile, W-band radar during VORTEX2. *Mon. Wea. Rev.*, **141**, 3661-3690.

Wakimoto, R. M., P. Stauffer, W.-C. Lee, N. T. Atkins, and J. Wurman, 2012: Finescale structure of the LaGrange, Wyoming, tornado during VORTEX2: GBVTD and photogrammetric analyses. *Mon. Wea. Rev.*, **140**, 2939-2958.

Weiss, C. C., D. C. Dowell, J. L. Schroeder, P. S. Skinner, A. E. Reinhart, P. M. Markowski, and Y. P. Richardson, 2015: A comparison of near-surface buoyancy and baroclinity across three VORTEX2 supercell intercepts. *Mon. Wea. Rev.* (in revision)

Wurman, J., D. Dowell, Y. Richardson, P. Markowski, E. Rasmussen, D. Burgess, L. Wicker and H. Bluestein, 2012: The second Verification of the Origin of Rotation in Tornadoes Experiment: VORTEX2. *Bull. Amer. Meteor. Soc.*, **93**, 1147-1170.

Wurman, J., K. A. Kosiba, and P. Robinson, 2013: In situ, Doppler radar, and video observations of the interior structure of a tornado and the wind-damage relationship. *Bull. Amer. Meteor. Soc.*, **94**, 835-8

Figure 1 – Photograph of the sampled tornado, near Rozel, KS at 0033 UTC (19 May 2013). Photo courtesy of the University of Michigan.

Figure 2 – Photograph of cyclic tornado development near Cherokee, OK on 14 April 2012. View is to the west-southwest. Photo credit: Tony Reinhart (TTU)

a)

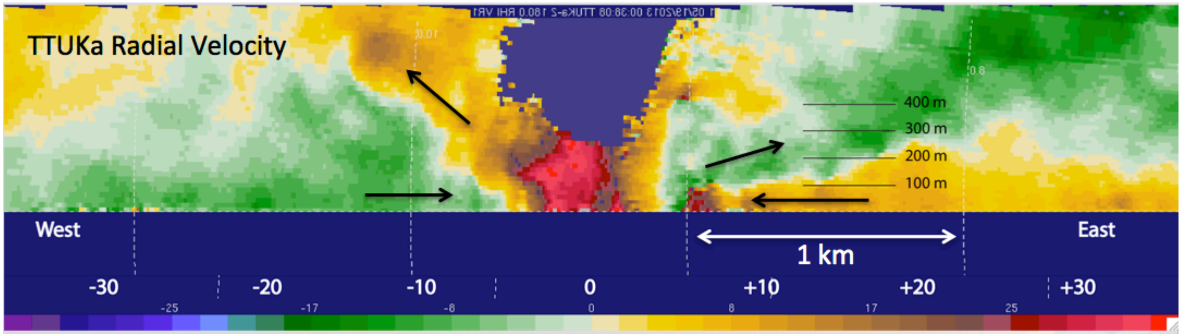

b)

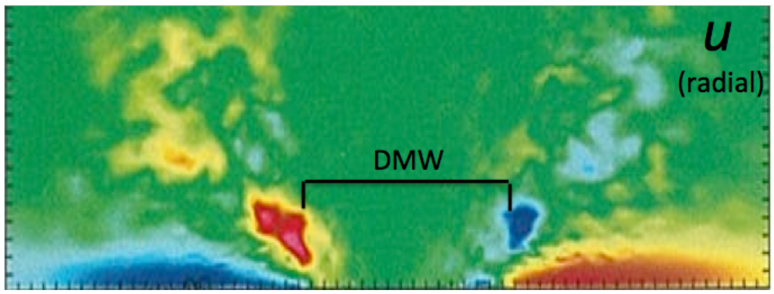

Figure 3 – (a) TTUKa-2 RHI radial velocity through the core of the Rozel, KS tornado, valid at 0038 UTC, 19 May 2013. Elevation is indicated. Black arrows are included to denote the sense of the vertical secondary circulation. (b) Radial velocity from a large eddy simulation of a tornado by Lewellen et al. (2000); reproduced in Markowski and Richardson (2010). The diameter of maximum wind (DMW) is denoted; the dimension of the figure is scaled to match the DMW in a). Velocity scale is included at the bottom of each figure.

a)

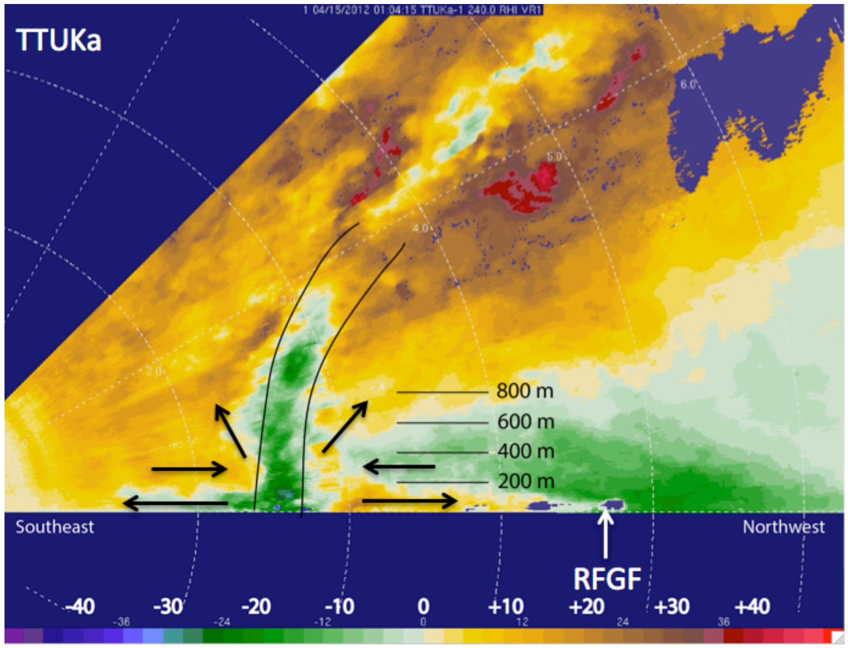

b)

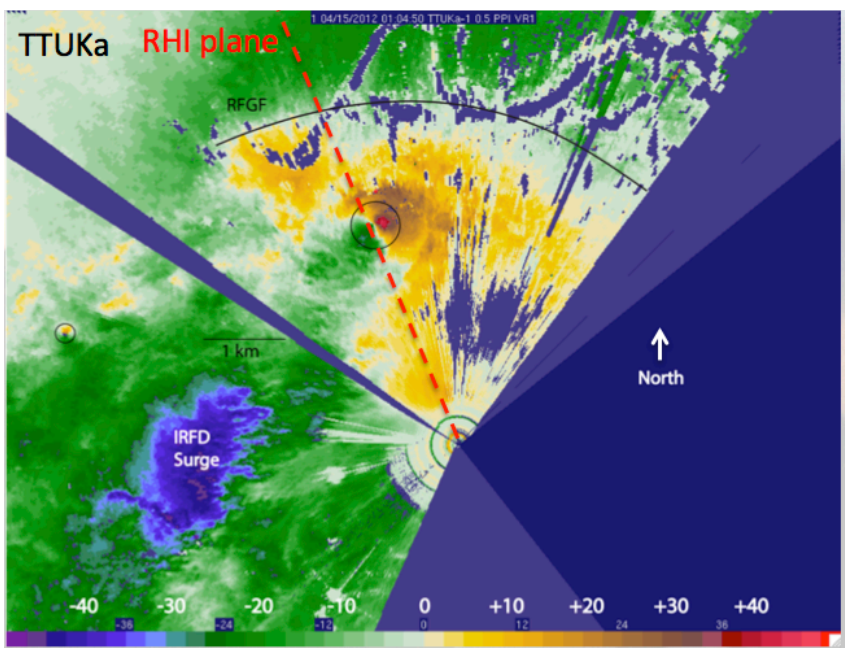

Figure 4 – (a) TTUKa-1 RHI of the core flow of the (second) Cherokee, OK tornado of 14 April 2012, valid at 0104 UTC (15 April). Elevation is indicated. The solid black contour denotes the weak echo region of the tornado. Black arrows are included to show the sense of the vertical secondary circulation. (b) 0.5 deg TTUKa-1 PPI of the (second) Cherokee, OK tornado, valid at 0105 UTC. The locations of the primary rear flank gust front (RFGF), internal RFD surge, RHI plane for (a) and tornadoes (circles) are indicated. Velocity scale is included at the bottom of each figure.

a)

b)

Figure 5 – Photographs of the (second) Cherokee, OK tornado of 14 April 2012, valid at (a) 0104:45 UTC and (b) 0106:30 UTC (15 April). View for the photographs is a) northwest and b) north-northwest.

a)

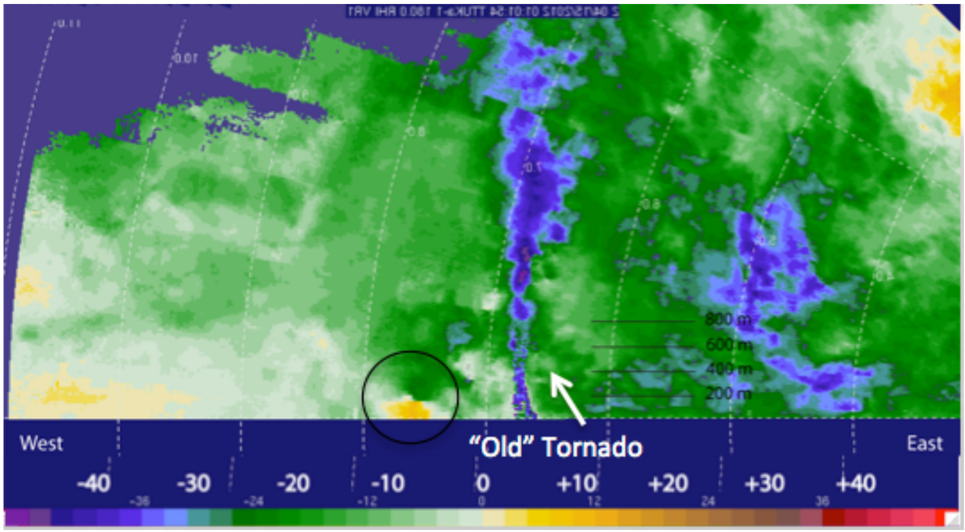

b)

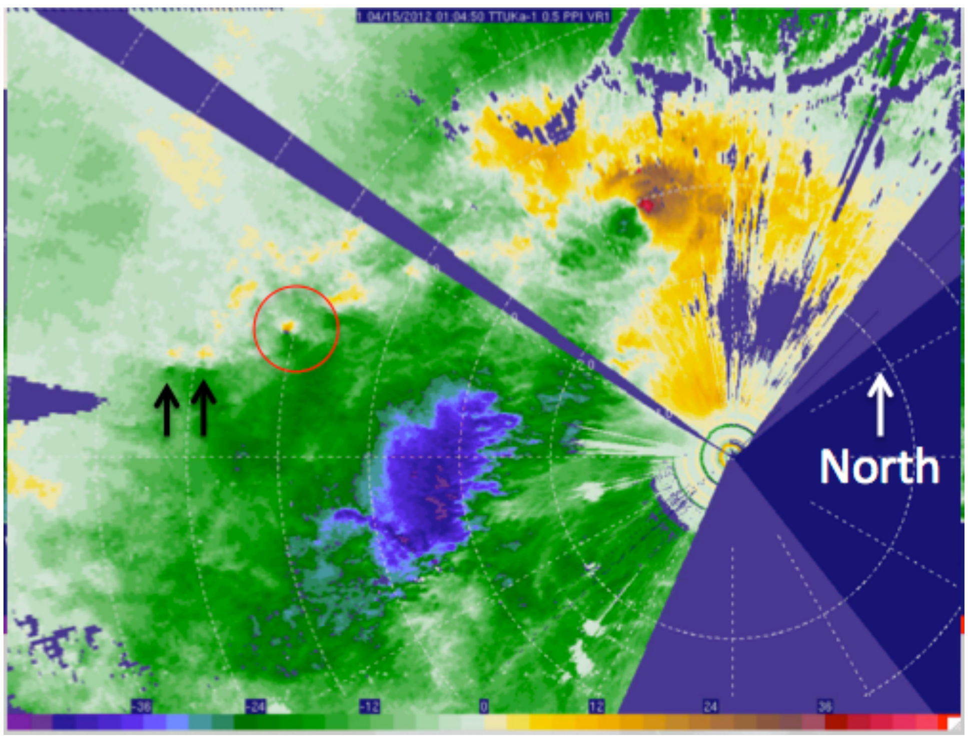

Figure 6 – (a) TTUKa-1 RHI of the (first) Cherokee, OK tornado and separate region of strong vorticity (circled), valid at 0102 UTC. (b) TTUKa-1 PPI valid at 0105 UTC, where the first tornado is circled in red and the black arrows denote separate weak vertical vorticity maxima trailing the tornado. Velocity scale is included at the bottom of each figure.